

Information supercurrents and spin waves in chiral active matter: Universality of the Landau-Lifshitz-Gilbert equation

Magnus F Ivarsen*

Department of Physics and Engineering Physics, University of Saskatchewan, Saskatoon, Canada

Recent minimalist modeling has demonstrated that overdamped polar chiral active matter can support emergent, inviscid Euler turbulence, despite the system's strictly dissipative microscopic nature. In this article, we establish the statistical mechanical foundation for this emergent inertial regime by deriving a formal isomorphism between the model's agent dynamics and the overdamped Langevin equation for disordered Josephson junctions. We identify the trapped agent state as carrying non-dissipative phase rigidity supercurrents, a mapping we confirm empirically by demonstrating a disorder-broadened Adler-Ohmic crossover in the system's slip velocity. Generalizing this framework to three dimensions ($S^1 \rightarrow S^2$), we show that the polar alignment interaction is geometrically equivalent to the Gilbert damping term in spintronics. This constraint naturally generates inertial spin waves (ferromagnetic magnons) from the overdamped active bath, recovering the macroscopic transport predicted by Toner-Tu theory without invoking microscopic inertia. These results classify chiral active matter as a dissipative spintronic fluid, revealing that the transition to active turbulence is the emergence of a topological quasiparticle gas, where macroscopic Onsager dipoles acquire effective inertia from the Goldstone modes of the underlying broken symmetry.

I. INTRODUCTION

Active turbulence describes the chaotic spatiotemporal dynamics observed across a diverse spectrum of living and synthetic matter. This phenomenon is ubiquitous in non-equilibrium systems, having been rigorously characterized in the dense, swirling collective motion of bacterial swarms [1, 2], the restructuring of subcellular cytoskeletal extracts [3], and the engineered flows of synthetic colloidal flocks [4, 5]. The hydrodynamic conditions under which these behaviors emerge represents a fundamental challenge to statistical physics. Unlike classical inertial turbulence, which strictly requires high Reynolds numbers (Re) to overcome viscosity and sustain energy cascades, active turbulence is overdamped ($Re \approx 0$). In this viscous regime, where flows are expected to be laminar, chaotic transport is instead sustained by a distinct mechanism: the continuous, non-conservative injection of energy at the microscale, which drives the system far from equilibrium [6, 7].

A recent minimalist, two-dimensional chiral active matter model offers a solution to the paradox by empirically demonstrating that an overdamped chiral flock can drive a conservative inertial cascade that culminates in inviscid Euler turbulence, in the form of a stable, sloshing Onsager dipole in the dynamic agent ensemble, where topological defects interact long-range through the Kirchoff-Onsager hamiltonian [8] (Figure 1). The present article provides detailed theoretical backdrop for the findings in Ref. [8].

As we shall demonstrate, the agent inertia that is engineered into several successful hydrodynamic models of chiral flocks [9–11] can be replaced by a natural synchro-

nization stiffness that mimicks an inertial flow, clearly observable in our minimalist model.

The model is characterized by three simple rules, namely that its agents are (1) self-propelled, (2) polar, or flocking, favoring alignment, and (3) chiral, with intrinsic rotation [8, 12]. The model is unique in that it collapses these three properties into a single degree of freedom, phase, ϕ_i ,

$$\dot{\mathbf{r}}_i = v_0 \hat{\mathbf{n}}(\phi_i), \quad (1)$$

where \mathbf{r}_i is an agent's position, v_0 its constant swim speed, and $\hat{\mathbf{n}}(\phi_i) = (\cos \phi_i, \sin \phi_i)$ is the polar unit vector for internal phase $\phi_i \in [0, 2\pi)$. The time evolution in phase is given by,

$$\dot{\phi}_i = \omega_i + a_0 R \sin(\Psi - \phi_i) + \eta_i(t), \quad (2)$$

where ω_i is an agent's intrinsic chirality, or *frustration*, $\eta_i(t)$ is a Gaussian white noise term, and $a_0 R \sin(\Psi - \phi_i)$ is a localized Kuramoto-Sakaguchi-coupling [13, 14]. With R being the local order parameter, we note that

$$\begin{aligned} Z(\mathbf{x}, t) &= R(\mathbf{x}, t) e^{i\Psi(\mathbf{x}, t)} = \\ &= \int_{\mathcal{D}} G(|\mathbf{x} - \mathbf{x}'|) \left[\sum_{j=1}^N \delta(\mathbf{x}' - \mathbf{x}_j(t)) e^{i\phi_j(t)} \right] d\mathbf{x}', \quad (3) \end{aligned}$$

is the local complex order parameter field, expressed as the convolution of the microscopic agent distribution with a finite-range interaction kernel $G(|\mathbf{x} - \mathbf{x}'|)$, representing attractive forces between agents that align. By defining a continuum field theory for Eqs. (2) and (3), Ref. [12] demonstrated that the ensemble of active agents is subject to a kinetic Turing instability, triggered by the interplay between Z (activation) and ω_i (inhibition).

Of some importance, Refs. [12] and [8] both explicitly considered a renormalized fluid element in the model, the

* Contact: magnus.fagernes@gmail.com; Also at The European Space Agency Centre for Earth Observation, Frascati, Italy

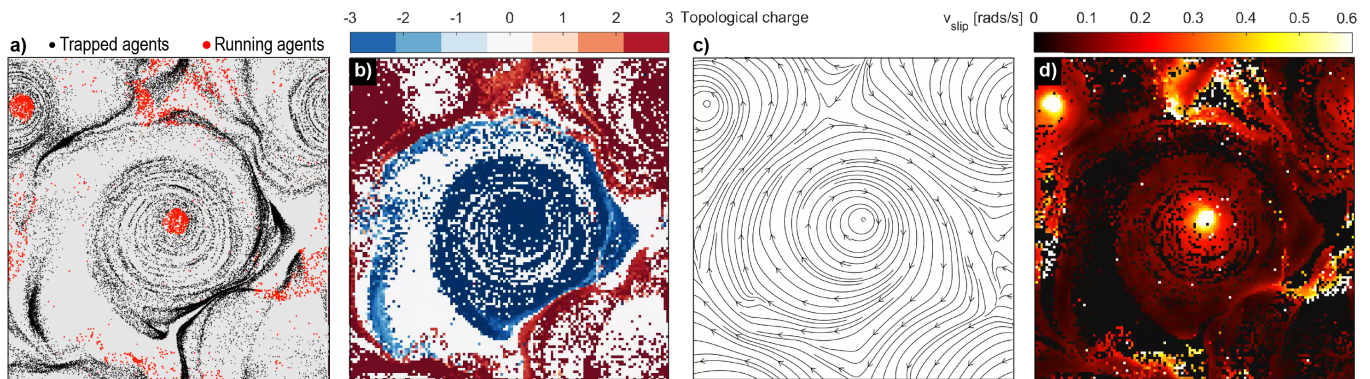


FIG. 1. **A simulated ensemble of polar chiral active matter agents.** Panels a–d) show end-state snapshots of the entire simulation space, with agent point-cloud (**panel a**), topological charge (**panel b**), flow-lines of circulation in order R^2 (**panel c**), and agent slip velocity v_{slip} (**panel d**), with respective colorscales where applicable. In panel a), trapped agents are shown in black while running agents are shown in red.

former by calculating the guiding centre location of each agent’s oscillatory motion, and the latter by the implementation of a low-pass filter scaled by the interaction correlation timescale. The papers motivated this step in terms of the Vlasov-Fokker-Planck equation [12] and shallow water theory [8], and, as we have stated, the latter rigorously demonstrated that Eqs. (2) and (3) thereby lead to inviscid Euler turbulence in the form of an *Onsager dipole*.

However, an important question remains. Our active agent ensemble is demonstrably overdamped and dissipative, yet the model exhibits an inverse, conservative energy cascade. How does a system that should fundamentally decay instead pump energy towards the largest scales? The resolution lies in considering the discrete distribution of agents as a spatially extended, disordered Josephson junction array. The depinning transition between ‘running’ and ‘trapped’ states then generates a macroscopic synchronization stiffness, or supercurrents of phase gradient information. By extending the model’s equations to three dimensions (3D), we eventually demonstrate that the rigidity supports Goldstone mode spin waves that map the two-dimensional (2D) model to the azimuthal precession of 3D active chiral agents. We shall contrast these ferromagnetic magnons against the second sound waves of the Toner-Tu field theory, delineating the universality of the Landau-Lifshitz-Gilbert equation.

II. THEORETICAL FOUNDATION

In chiral flocks, motile agents that possess polar symmetry and seek to align, phenotypic heterogeneity [15] produces an intrinsic frequency dispersion among the flock constituents, in much the same way that semiconductor fabrication introduces a dispersion in the superconductor chips called Josephson junctions [16, 17]. Josephson junctions are essentially ensembles of quantum

oscillators with a non-zero dispersion $\Delta\omega$ in their natural frequencies ω_i , that synchronize (phase-lock) via a collective (global) coupling K if the coupling strength is able to overcome the ensemble’s fabrication heterogeneity, or dispersion, $\Delta\omega$. Crucially, the coupling K is naturally described with the Kuramoto-model [18], readily providing a theoretical foundation to understand the thermodynamics of our minimal model, which features a long-range, locally mediated Kuramoto interaction (Eqs. 2, 3).

In this letter, we shall consider Eq. (2) as the overdamped Langevin equation, following Ref. [19], which leads to the tilted washboard potential [17]. Given that our model’s agents are essentially massless, we shall derive a formal mapping to the *resistively shunted junction* model in the overdamped limit [20, 21].

We begin by writing Eq. (2) as,

$$\dot{\phi}_i = -\frac{\partial V_{\text{eff}}}{\partial \phi_i} + \eta_i(t), \quad (4)$$

where,

$$V_{\text{eff}}(\phi_i) = -a_0 R \cos(\Psi - \phi_i) - \omega_i \phi_i, \quad (5)$$

is the classic tilted washboard potential characterized by two competing energy scales, the potential wells $a_0 R$ (which synchronize agents), and the tilt ω_i (which desynchronize agents).

In this dynamic, the stochastic noise $\eta_i(t)$ and the intrinsic frequency dispersion in ω_i function as sub-gap leakage [22, 23] driving the irreducible background entropy production described by Ref. [24]. This continuous dissipation ensures that the emergent inertial fluid retains a finite ‘thermal viscosity’ that prevents the system from freezing into a glass-state, even deep within the phase-locked regime. This mechanism establishes a direct isomorphism to Ref. [25], which demonstrated that the 2D topology of an inherently disordered Josephson array allows for coherent microwave emissions despite significant microscopic inhomogeneity (see also Ref. [26]).

To characterize the thermodynamics of Ref. [8]’s fluid-theoretically derived “shock cycle” between the active, dissipative bath and an ordered, inertial state, we shall derive an agent’s phase velocity in the co-moving Lagrangian frame of the local order parameter. We start by decomposing an agent’s phase velocity,

$$\phi_i(t) = \Psi_i(t) + \delta\phi_i(t), \quad (6)$$

where $\Psi_i(t) = \Psi(\mathbf{r}_i(t), t)$ is the local phase at agent i ’s location, representing the collective phase evolution, and $\delta\phi_i(t)$ represents an agent’s relative phase evolution. Taking the time derivative of Eq. (6) yields,

$$\dot{\phi}_i = \dot{\Psi} + \dot{\delta\phi}, \quad (7)$$

from which we define,

$$v_{\text{slip}} \equiv |\delta\dot{\phi}_i| = |\dot{\phi}_i - \dot{\Psi}_i|, \quad (8)$$

as an agent’s phase slip velocity. Here, we identify $\dot{\phi}_i$ as an agent’s deterministic phase velocity (Eqs. 2, 5) and $\dot{\Psi}_i$ as the phase velocity of the potential well seen by that agent, meaning that v_{slip} represents an agent’s phase speed relative to a potential well. By quantifying v_{slip} (Eq. 8) we can therefore measure whether an agent is being thermalized into the active bath, or whether it is contributing to an inertial Euler flow in R^2 [8].

This realization allows us to pinpoint the mathematical isomorphism that explains why the system bifurcates into a hydrodynamic (trapped) state and an active bath (running) state. We use Eq. (2) deterministically to rewrite Eq. (7) in form of,

$$\delta\dot{\phi}_i = \omega_i - \dot{\Psi}_i - a_0 R \sin \delta\phi, \quad (9)$$

which is, *in exact terms*, the Adler equation [27, 28] for a dirty, or disordered, Josephson array [18], with individual junctions driven by an effective current I_{eff} [22],

$$I_{\text{eff}} = \omega_i - \dot{\Psi}_i. \quad (10)$$

Here, we identify $\Delta\omega$,

$$\langle \omega_i - \dot{\Psi}_i \rangle = \Delta\omega, \quad (11)$$

the dispersion in the agents’ intrinsic frequency, corresponding to inertial fluid’s *topography* in the shallow water isomorphism derived in Ref. [8]. Consistent with this inference, the effective current in Eq. (10) is a driving force that tries to break local synchronization. Setting Eq. (9) to zero and solving for $\delta\phi$ yields the critical current,

$$I_c = a_0 R, \quad (12)$$

which likewise follows from considering the potential well depths in the tilted washboard potential (Eq. 5). When $|I_{\text{eff}}| < I_c$, the local coupling force $a_0 R$ is strong enough to trap the agent, which subsequently locks onto a stable

fixed angle and swims with the local group. Conversely, when $|I_{\text{eff}}| > I_c$, the agent’s intrinsic frustration exceeds the local maximum coupling force. The agent runs or slips relative to the group, with the phase continuously rotating.

In equivalent terms, for Josephson junctions, when $I_{\text{eff}} < I_c$ an oscillator famously locks onto a constant value. However, whereas the critical current of a Josephson junction depends on material qualities, $I_c = a_0 R$ is in the present model *entirely dynamic* and depends on local synchronization. Still, we observe complete isomorphism between Eq. (9) and the Adler equation for a Josephson junction with in-series resistance [22]. When $I_{\text{eff}} > I_c$ the Josephson junction cannot hold onto the phase, acquires a voltage, and subsequently produces entropy through dissipative currents. Equivalently, in our model, when an agent runs or slips relative to the group, it acquires the voltage,

$$V_{\text{eff}} = |\dot{\phi}_i - \dot{\Psi}_i| = v_{\text{slip}}. \quad (13)$$

The resistive motion of the agent then thermalizes energy into the active bath.

We can thus formalize Ref. [8]’s description of the model’s central thermodynamic process; when agents start to slip, R drops, lowering the local critical current I_c . This causes neighbours to slip, forcing a cascade in energy, resulting in a locally disorganized state ($R \approx 0$). However, this state is linearly unstable to the kinetic Turing instability [12]. Once agents have thermalized, they re-organize. In the tilted washboard formalism, as R grows, the potential wells deepen, drawing more agents in. Their intrinsic rotation ω_i is now synchronized by spatial segregation, producing a distinct *topography* for the inertial flow [8].

Following Ref. [22]’s demonstration of how individual Josephson oscillators respond to external forcing, we calculate the time required for a 2π phase slip,

$$T_{\text{slip}} = \int_0^{2\pi} \frac{d\delta\phi}{\dot{\delta\phi}} = \frac{2\pi}{\sqrt{I_{\text{eff}}^2 - I_c^2}}, \quad (14)$$

where we inserted the Adler equation into the integral (Eq. 9). Consequently, the instantaneous slip velocity is

$$v_{\text{slip}} = \frac{2\pi}{T_{\text{slip}}} = \sqrt{I_{\text{eff}}^2 - I_c^2}, \quad (15)$$

where we note that whereas Eq. (8) measures an agent’s realized slip velocity, Eq. (15) provides a theoretical prediction for the slip velocity based on the established response function of an ideal Josephson junction; the convergence of the two at high disorder will provide empirical weight behind our central thesis.

Examining the asymptotic limits of Eq. (15) reveals two distinct dynamical regimes in the deterministic limit (see also Ref. [29]):

$$v_{\text{det}} = \begin{cases} \sqrt{I_{\text{eff}}^2 - I_c^2} \sim \sqrt{I_{\text{eff}} - I_c} & \text{for } I_{\text{eff}} \geq I_c \\ 0 & \text{for } I_{\text{eff}} < I_c \end{cases} \quad (16)$$

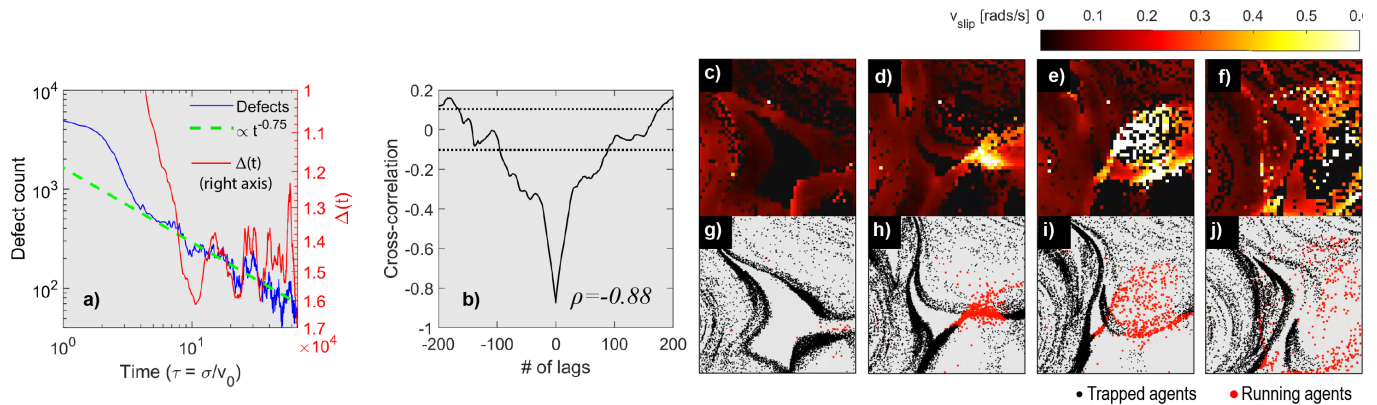


FIG. 2. **Panel a)** shows defect count as a function of normalized simulation time (left y -axis) with a $t^{-0.75}$ powerlaw fit shown with a green, dashed line, and the average potential barrier height $\Delta(t)$ (Eq. 18) in red (right y -axis, inverted). **Panel b)** shows a cross-correlation analysis of the latter two timeseries, for normalized times > 5 . Estimated confidence intervals for the cross-correlation are shown with dashed, black lines. **Panels c–j)** show inset v_{slip} and trapped/running agent pointclouds, data from the black square in Figure 1d, in rapid succession-snapshots, highlighting ongoing shock merger, agent thermalization, and subsequent re-organization. See Video S1 in the Supplementary Materials for a video of this simulation run.

In equivalent terms, we follow Ref. [22]’s formalism for single junctions, adapting it for the ensemble average, $\langle v_{\text{slip}} \rangle$, obtained by integrating Eq. (15) over the probability distribution $P(I_{\text{eff}})$. This accounts for noise as a fluctuating tilt that statistically drives the system across the critical threshold:

$$\langle v_{\text{slip}} \rangle = \int_{|I_{\text{eff}}| > I_c} P(I_{\text{eff}}) \sqrt{I_{\text{eff}}^2 - I_c^2} dI_{\text{eff}}. \quad (17)$$

Eq. (17) is expected to conform to the specific ‘soft knee’ geometry identified in Ref. [22] and stands in direct correspondence with Ref. [18], which established that the macroscopic resistance of a disordered Josephson array scales with the fraction of running junctions, demarcating the phase transition from a ‘superconducting glass’ (pinned, or trapped, phases) to a resistive metal (running phases).

In what follows, we demonstrate that our minimal active matter model effectively realizes a motile Josephson array. By embedding the discrete oscillator dynamics of Ref. [22] into intrinsically motile (self-propelled) agents, we introduce a transport mechanism absent in standard static arrays [18]. In our model, dissipative excitations are physically advected by the running agents themselves. This active transport expels disorder from the ordered bulk and concentrates it into defect cores, segregating the system into a dual-phase fluid. The segregation mimics the thermodynamic state preparation observed in driven optical systems [26], where the *interplay of drive and dissipation stabilizes distinct macroscopic phases* (see also Refs. [25, 30]). Specifically, we observe (1) an ideal, inviscid Euler fluid of *trapped* agents with inertial mass proportional to order squared [8], and (2) a dissipative resistive fluid of *running* agents. This resistive phase acts as the thermodynamic sink that ultimately sustains the cycle, permitting the regeneration of order via a kinetic Turing instability [12].

III. EMPIRICAL RESULTS

We have implemented the model (Eqs. 2, 3) in a bounded periodic box with $N = 50,000$ agents, akin to Refs. [8, 12]. Figure 1 presents snapshots of the fully formed Onsager dipole, with panels a–c) showing agent point cloud, topological charge, and inertial flowlines, respectively. Panel d) shows the slip velocity v_{slip} (Eq. 8), for the entire simulation space.

Figure 2c–j), showing four prior v_{slip} -snapshots of a limited portion of the simulation space, offer an instructional explanation of the model’s core thermodynamic mechanism. An ordered ($R \approx 1$) region shatters into phase slips (active turbulence), generating entropy; this is the shock merger mechanism identified by Ref. [8]. The agents inside this now-disordered patch are then quickly reorganized into the inertial fluid by the kinetic Turing instability [12].

Figure 2a, b) demonstrate the foregoing dynamic in rigorous terms. First, we define the gap excess $\Delta(t)$, a metric derived from the potential barrier height of the overdamped Adler equation [22]. That is, we sum the potential heights for the trapped population,

$$\Delta(t) = \sum_{\text{trapped}} \left(a_0 R - |\omega_i - \dot{\Psi}_i| \right), \quad (18)$$

where the argument t indicates that the quantity is a timeseries. $\Delta(t)$ thus measures the sum total depths of the local potential wells [19] (\mathcal{U}_B , termed potential barrier height in Ref. [22]) that confine each trapped agent’s phase.

Figure 2a) shows topological defect count going down with a characteristic scaling of $t^{-0.75}$ [31, 32], identified by Ref. [8] to be caused by shock dynamics. At the same time, and with a strong negative correlation coefficient of -0.88 (Figure 2b), the gap excess $\Delta(t)$, or locking

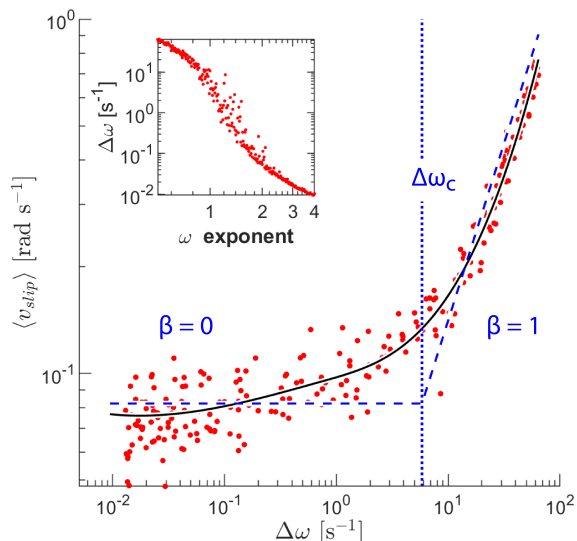


FIG. 3. The result of 256 simulations systematically varying the exponent in the ω_i distribution, yielding a systematically varied disorder strength $\Delta\omega$ (keeping the peak of the ω_i unchanged at 0.2 s^{-1} , $\Delta\omega$ is calculated using the standard deviation), shown in the inset panel. The main plot shows observed ensemble average of the slip velocity $\langle v_{\text{slip}} \rangle$ (voltage) against dispersion $\Delta\omega$ (current), in a log-log “I-V” plot. $\langle v_{\text{slip}} \rangle$ is calculated as the mean value of v_{slip} for all N agents, collected during four snapshots of the second half of each simulation. A solid black line shows a 4th order Hermite polynomial fit [33], while a dashed-blue line shows a 2nd order (piece-wise linear) Hermite polynomial fit with slopes (exponent β) of 0 and 1. A vertical blue-dotted line indicates the theoretical mean-field critical threshold dispersion, $\Delta\omega_c \approx 6 \text{ s}^{-1}$. The observable onset of slip velocity occurs significantly earlier (around $\Delta\omega \approx 0.5 \text{ s}^{-1}$), indicating substantial sub-gap leakage current driven by the intrinsic disorder of the array.

strength of the trapped agents [22], increase. The rise in $\Delta(t)$ during shock mergers confirms the topological heat pump mechanism: the annihilation of resistive defects ($\mathcal{U}_B \approx 0$) instantaneously throws agents into deep superconducting traps ($\mathcal{U}_B \gg 0$), actively lowering the system’s effective phase temperature.

The I-V Curve

Next, we shall provide definite empirical evidence for our thesis by systematically varying total agent disorder, termed dispersion in Refs. [8, 12]; that is, $\langle I_{\text{eff}} \rangle = \Delta\omega$ (Eq. 11), in successive simulations, essentially implementing a Monte-Carlo simulation of the current-voltage (I-V) curve for our model. Here, we note that $\Delta\omega$ is entirely decided by the exponent n of the powerlaw distribution in ω_i ; $P(\omega) \sim \omega^{-n}$ [8, 12]. We therefore systematically vary n from 0.5 to 4. Figure 3 shows the result in a scatterplot of the ensemble-averaged slip velocity $\langle v_{\text{slip}} \rangle$ against $\Delta\omega$, aggregating 256 simulations. To characterize the macroscopic response function without imposing the

rigid constraints of a single-parameter junction model, we fit $\langle v_{\text{slip}} \rangle$ using a shape-preserving 4th-order Hermite polynomial [33] (solid black line). This phenomenological approach accommodates the inhomogeneous broadening caused by the structural disorder of the agent array [22].

Crucially, the solid-black fit in Figure 3 reveals a continuous evolution of the local scaling exponent. At very low dispersion ($\Delta\omega \ll \Delta\omega_c$), the response is dominated by a noise floor ($\beta = 0$), gradually rising towards $\Delta\omega_c \approx 6 \text{ s}^{-1}$. The gradual rise in $\langle v_{\text{slip}} \rangle$ towards 6 s^{-1} is consistent with sub-gap leakage currents smoothing out the $\beta = 0.5$ transition [22]. As the dispersion exceeds the critical threshold, $\Delta\omega > \Delta\omega_c$, the system quickly and strictly adheres to a linear regime, asymptotically recovering the Adler-Ohmic limit ($\beta = 1$).

The classification of the minimal model as a disordered Josephson array is empirically demanded by the system’s macroscopic response function (Figure 3), which traverses the distinct Adler-Ohmic crossover predicted by the resistively shunted junction formalism [18, 29] with the disorder-induced rounding identified in Ref. [22], a signature of the Adler equation’s saddle-node bifurcation. This distinguishes the model’s central mechanism from standard viscous fluid transitions and justifies the identification of a tilted washboard potential [19]. The subsequent recovery of the linear Ohmic limit ($\beta = 1$) at high-disorder confirms that Ref. [8]’s characterization of the model’s emergent, inertial superfluid is rigorously predicted by the non-linear phase topology of disordered oscillator arrays.

IV. RECONCILING THE MODEL WITH REAL, THREE-DIMENSIONAL CHIRAL FLOCKS

The foregoing established experimental proof of the Adler mechanism in our minimal model. However, the derived supercurrents of state information are *maintaining* order in the chiral flock. In realistic flocks, ‘second sound’ waves propagate through this ordered ensemble [9]. Is our overdamped chiral model able to reproduce realistic flocking behaviour?

By increasing the degrees of freedom from 1 to 2, we can shift from the two-dimensional, minimal model to the real, three-dimensional dynamics of polar chiral flocs ($S^1 \rightarrow S^2$), illustrated in Figure 4. Eqs. (1, 2) map a scalar phase ϕ_i to a two-dimensional \mathbf{r}_i . In three dimensions, the agent state becomes a unit phase vector $\hat{\mathbf{n}}_i$ on the unit sphere S^2 . The agent’s position is then $\mathbf{r}_i = v_0 \hat{\mathbf{n}}_i$, with $|\hat{\mathbf{n}}_i| = 1$ (Figure 4b). The local order parameter $Z = R e^{i\Psi}$ (Eq. 1) becomes a local director field vector $\mathbf{R} = R \hat{\Psi}$, where $\hat{\Psi}$ is the mean direction of the local neighborhood and R is the coherence magnitude.

Next, to express the Adler dynamics (Eq. 9), we note that ω_i (intrinsic rotation) becomes an intrinsic angular velocity vector $\boldsymbol{\omega}_i$. With this, the coupling term $a_0 R \sin(\Psi - \phi_i)$ represents a torque trying to align \mathbf{n}_i with Ψ (expressed as $\hat{\mathbf{n}}_i \times \hat{\Psi}$). To keep the overdamped nature

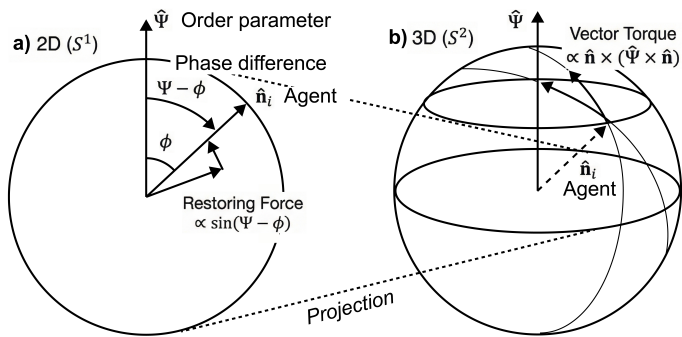


FIG. 4. **Panel a)**: the geometry of the 2D model, showing how the restoring force acts to align an agent's phase ϕ with the mean field Ψ . **Panel b)**: the geometry of the 3D extension, where orientation is the unit vector on a spherical surface ($|\hat{\mathbf{n}}_i| = 1$), and where the vector torque proportional to $(\hat{\mathbf{n}}_i \times \hat{\Psi}) \times \hat{\mathbf{n}}_i$ (Eq. 19) acts to align the agent with the mean field, and represents spin relaxing to align with a magnetic field [34]. This vector torque projects to the restoring force in panel a).

of the model, we then take a small-angle approximation of the angular velocity (near 0), yielding an inertia-less, linear expression (angular velocity \propto torque). After this, we can express the equation of motion for an agent i as,

$$\frac{d\hat{\mathbf{n}}_i}{dt} = (\boldsymbol{\omega}_i \times \hat{\mathbf{n}}_i) + a_0 R (\hat{\mathbf{n}}_i \times \hat{\Psi}) \times \hat{\mathbf{n}}_i + \boldsymbol{\eta}_i(t), \quad (19)$$

where we recognize the first term as intrinsic agent chirality, or frustration, and the second term as the localized Kuramoto-alignment term (Eq. 2). Here, we note that, in the spintronics of spin waves (ferromagnetic magnons), where the phase vector stays on the unit sphere (Landau-Lifshitz-Gilbert damping form [34, 35]), $\hat{\mathbf{n}}_i$ effectively relaxes towards $\hat{\Psi}$ (Figure 4b).

The angular velocity being strictly proportional to the applied torque allows for the gyroscopic damping by the energy of the dissipative system continuously decreasing, entirely equivalent with the washboard's potential wells in the the two-dimensional description (Figure 5), and entirely aligned with the damping term in the Landau-Lifshitz-Gilbert spintronics [34].

The decomposition of phase into a co-moving term with a perturbation (Eq. 6), which led to the Adler equation in the two-dimensional case (Eq. 9), now needs angular velocity $\boldsymbol{\Omega}_\Psi$, defined as,

$$\frac{d\hat{\Psi}}{dt} = \boldsymbol{\Omega}_\Psi \times \hat{\Psi}, \quad (20)$$

after which the natural definition of a slip vector $\boldsymbol{\Omega}_{slip}$ becomes,

$$\left. \frac{d\hat{\mathbf{n}}_i}{dt} \right|_{slip} = \boldsymbol{\Omega}_{slip} \times \hat{\mathbf{n}}_i. \quad (21)$$

Subtracting the frame rotation $\boldsymbol{\Omega}_\Psi$ from the agent's total

motion yields the vector expression of Eq. (15),

$$\boldsymbol{\Omega}_{slip} = \underbrace{(\boldsymbol{\omega}_i - \boldsymbol{\Omega}_\Psi)}_{\equiv \mathbf{I}_{eff}} - \underbrace{a_0 R (\hat{\Psi} \times \hat{\mathbf{n}}_i)}_{\equiv \mathbf{I}_c}. \quad (22)$$

That is, the minimal agent dynamics mapping a two-dimensional unit phase vector to a three-dimensional unit vector naturally leads to an Adler relation. Remarkably, this occurs without the explicit definition of a Kuramoto-term. The reason for this stem from the recognition of the Landau-Lifshitz-Gilbert-equation from ferromagnetic theory, where a spin \mathbf{S} naturally relaxes towards a magnetic field \mathbf{H} (Figure 4b). The three-dimensional synchronization in a chiral flock described in Eqs. (19) is therefore equivalent to magnetic damping.

Mathematically, the three-dimensional definitions preserved the symmetry group of the interaction while lifting the dimensionality, from which Kuramoto synchronization emerges without the ansatz.

Finally, we can derive a locking condition in three dimensions. The scalar slip velocity v_{slip} defined in Eq. (8) becomes the magnitude of the slip vector: $v_{slip}^{3D} \equiv \|\boldsymbol{\Omega}_{slip}\|$, and setting this scalar equal to zero requires the effective driving current \mathbf{I}_{eff} to be perfectly balanced by the restoring torque,

$$\boldsymbol{\omega}_i - \boldsymbol{\Omega}_\Psi = a_0 R (\hat{\Psi} \times \hat{\mathbf{n}}_i). \quad (23)$$

Taking the magnitude of both sides yields,

$$\|\boldsymbol{\omega}_i - \boldsymbol{\Omega}_\Psi\| = a_0 R |\sin(\theta)|, \quad (24)$$

where θ is equivalent to the angle between the agent and the flock $\delta\phi$ in Eq. 6). Since the maximum value of $|\sin(\theta)|$ is 1, we recover the exact Josephson inequality,

$$\|\mathbf{I}_{eff}\| \leq a_0 R. \quad (25)$$

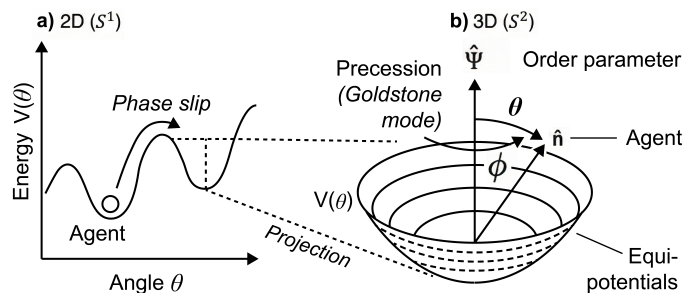


FIG. 5. **The tilted washboard potential.** **Panel a)**: the S^1 potential wells $V(\theta)$ of the tilted washboard potential, traversed by phase mismatch θ . **Panel b)**: the S^2 potential wells, where potential energy $V(\theta) \propto -\cos\theta$ is independent of the azimuthal angle ϕ , which means that the potential projects onto S^1 in mismatch θ . This enables effortless precession around the mean field and directly activates the Goldstone mode dynamics (Eq. 46); a quasiparticle that advects phase gradients (turning stiffness), thereby mimicking inertial mass.

The derivation of the vector Adler relation (Eq. 22) and the threshold critical current inequality (Eq. 25 from the S^2 constraint (Eq. 19) ensures that the phase locking behaviour of the two-dimensional Josephson junctions remains intact. As we shall derive in the next section, the phase-locked 3D chiral flock recess azimuthally, creating a Goldstone mode (topological quasiparticle).

V. OVERDAMPED SPIN WAVES AS ‘SECOND SOUND’ IN TONER-TU THEORY

The previous section established a three-dimensional adherence to the Adler equations, where flock synchronization naturally arises from a Kuramoto-like torque forced by the geometry of S^2 (Eq. 19). Having established the rigidity of the flock, the natural next step is to demonstrate that the predicted effects are observable in real 3D flocks. To do so, we must reconcile the 3D extension of our minimalist model with the standard model invoked to explain flocking in three dimensions: the Toner-Tu framework [9]. We begin with the 3D equations of motion, Eq. (19). To study the stability of the ordered state, we simplify by neglecting the intrinsic chirality ω_i , focusing on strong alignment:

$$\frac{d\hat{n}_i}{dt} = a_0 R (\hat{n}_i \times \hat{\Psi}) \times \hat{n}_i. \quad (26)$$

We examine the continuum limit $\hat{n}_i \rightarrow \hat{n}(\mathbf{r}, t)$, approximating the local order parameter $\hat{\Psi}$ as the director field plus a Laplacian correction:

$$\hat{\Psi} \rightarrow \hat{n} + \xi^2 \nabla^2 \hat{n}, \quad (27)$$

where ξ is the characteristic interaction scale. This approximation follows from the definition of $\hat{\Psi}$ as the average director within an interaction radius σ . Treating the agent distribution as a continuum, $\hat{\Psi}(\mathbf{r})$ is the convolution of $\hat{n}(\mathbf{r})$ with a local weighting kernel. A Taylor expansion of $\hat{n}(\mathbf{r} + \boldsymbol{\delta})$ averaged over an isotropic neighborhood eliminates first-order gradient terms ($\langle \boldsymbol{\delta} \rangle = 0$). The leading-order correction is therefore the quadratic term, proportional to $\nabla^2 \hat{n}$, which encodes the local field curvature. Consequently, ξ^2 scales with the square of the interaction radius ($\xi \sim \sigma^2$). Substituting these continuum relations into the alignment term of Eq. (26) yields:

$$\begin{aligned} (\hat{n} \times \hat{\Psi}) \times \hat{n} &\approx (\hat{n} \times (\hat{n} + \xi^2 \nabla^2 \hat{n})) \times \hat{n} = \\ &= (\hat{n} \times \xi^2 \nabla^2 \hat{n}) \times \hat{n}. \end{aligned} \quad (28)$$

Using the identity $(\mathbf{A} \times \mathbf{B}) \times \mathbf{C} = (\mathbf{A} \cdot \mathbf{C})\mathbf{B} - (\mathbf{B} \cdot \mathbf{C})\mathbf{A}$, we obtain the continuum overdamped equation:

$$\frac{\partial \hat{n}}{\partial t} = -(a_0 R \xi^2) \hat{n} \times (\hat{n} \times \nabla^2 \hat{n}). \quad (29)$$

This form is physically significant as it mirrors the dissipative damping term $\hat{n} \times (\hat{n} \times \mathbf{H})$ found in the Landau-Lifshitz-Gilbert equation of spintronics [34]. To fully capture the wave-like transport observed in Toner-Tu theories [9], we restore the inertial term neglected in the

overdamped limit. We introduce a coefficient of turning inertia, or precession stiffness, γ :

$$\frac{\partial \hat{n}}{\partial t} = -\gamma \hat{n} \times \nabla^2 \hat{n} - (a_0 R \xi^2) \hat{n} \times (\hat{n} \times \nabla^2 \hat{n}). \quad (30)$$

We note that this restoration of effective inertia is physically mandated by the conservation of angular momentum density: as the local order parameter R vanishes, the collective moment of inertia disappears ($I_{eff} \propto R$), compelling the precession rate to diverge to sustain a finite interaction torque. This description remains valid only while the local timescale separation persists, breaking down precisely at the defect cores ($R \rightarrow 0$) where the divergence signals the transition from a hydrodynamic superfluid to a strictly microscopic, overdamped gas. To satisfy dimensional consistency ($[\gamma] = L^2 T^{-1}$) within this physical constraint, we define the inertial coefficient as:

$$\gamma = \frac{a_0 \xi^2}{R}, \quad (31)$$

which leads to a direct mapping to the sound speed of the topological gas, $c_s \approx v_0 R$,

$$c_{\text{eff}} = v_0 \sqrt{\frac{K_{\text{torque}}}{\gamma}} = v_0 R, \quad (32)$$

where $K_{\text{torque}} = a_0 \xi^2 R$.

Physically, the inverse dependency in Eq. (31) implies that at the flock boundary ($R \rightarrow 0$), as alluded to, the precession frequency diverges. The system transitions from a ‘‘heavy,’’ locked superfluid in the bulk to a massless, fast-spinning gas at the edges. This divergence creates the active bath required to sustain the topological protection of the inner Onsager dipole [8].

The dispersion relation

By linearizing the polarized case (see Appendix A), the resulting spin waves are described, yielding the final total dispersion relation,

$$\omega(k) = \pm \frac{a_0}{R} k^2 - i(a_0 R) k^2. \quad (33)$$

The real part ($\pm a_0 R^{-1} k^2$) represents spin waves (ferromagnetic magnons), which diverge in frequency as the turning inertia vanishes ($R \rightarrow 0$). The imaginary part ($-i a_0 R k^2$) represents diffusive relaxation and vanishes in the disordered limit, confirming that the ordered flock is a rigid, wave-supporting medium [9] surrounded by a chaotic, fast-relaxing bath.

The active, 3D, overdamped bath on the boundaries of a real chiral flock naturally leads to a conservative azimuthal turning inertia of a spintronic fluid [34], by merit of the dimensional constraints of chiral alignment alone. The conservative fluid forms the characteristic flocking

behaviour, and is strictly contingent on the agents individually adhering to the phase-locking condition from Josephson junction theory (Eq. 25). The conservation is the relaxation of the stress-energy of the sphere S^2 , giving a geometric and thereby completely natural definition of synchronization in any system with polar alignment, by merit of the Landau-Lifshitz-Gilbert equation equation.

VI. DISCUSSION

A. Superconductivity

The recovery of strict disordered Josephson junction theory in the model equations follows from the alignment term $a_0 R \sin \delta\phi$ in our model being mathematically indistinguishable from the Josephson energy $E_J \sin \psi$. This phase rigidity enables information supercurrents that are sustained by agents trapped in a tilted washboard potential, analogous to Cooper pair supercurrents [36]. In Figure 3, we provide robust empirical evidence that the minimalist, two-dimensional model describes disordered, resistively shunted Josephson junctions [18, 22], capable of supporting supercurrents, which, as we shall defend with some rigour, facilitate a Goldstone mode-mediated transfer of phase gradients (rigidity) across an ensemble of polar chiral agents, carrying the topological protection of the bulk order.

However, in simpler terms, the supercurrents are the collective azimuthal rotation rate around the mean field of the spintronic fluid.

B. Thermodynamic pump

To see why, we identify the azimuthal angle of the S^2 potential as the scalar phase ϕ in the reduced S^1 limit. This degree of freedom is driven by the intrinsic chirality ω_i [and stochastic noise $\eta_i(t)$], providing the essential "frustration" mandated by Ref. [24] that prevents the chiral flock from freezing into a trivial, fully organized state. Instead, the frustration fuels a continuous, natural precession within the washboard potential wells (Figure 5b), generating the Goldstone mode quasiparticles (magnons) that sustain the fluid's inertia.

The two-dimensional model (Eqs. 2, 3, Figure 1) must therefore be taken to account for the tangent plane dynamics of the full 3D spintronic fluid. Crucially, this constraint identifies the physical origin of the system's inertia as the Landau-Lifshitz-Gilbert equation [34]; just as a gyroscope resists reorientation due to angular momentum, the chiral flock resists flow curvature due to the conservation of this azimuthal precession.

Inside the two-dimensional Onsager dipole's vortex cores, we observe in Figure 2a,d) that the agents are continuously phase-slipping. These cores are identified by Ref. [8] as massless ($R \rightarrow 0$) sonic black holes. In this limit, the critical current Eq. (12) vanishes, reducing the

Adler equation to its trivial kinematic limit ($\dot{\phi}_i \approx \omega_i$), and the spintronic fluid's capacity to support spin waves diverges, $\gamma \propto R^{-1}$ (Eq. 31). Consequently, the vortex cores are purely dissipative singularities where the capacity to sustain supercurrents has collapsed. This decoupling renders the cores unable to transmit phase stiffness or radiate coherent modes in the shallow water formalism, effectively silencing them within the inertial fluid.

C. Ferromagnetic magnons

In the inertial bulk, consisting of phase-locked agents that precess around the mean-field, the Goldstone mode yields spin waves in the form of ferromagnetic magnons. We derived the dispersion relation (Eq. 46),

$$\omega(k) = \pm \frac{a_0}{R} k^2 - i(a_0 R) k^2.$$

We make the following two key observations:

(1) the real part of $\omega(k)$ corresponds to the conservative propagation of phase gradients ('trapped' supercurrents) that provide the Euler-like inertia, while the imaginary component captures the inevitable sub-gap leakage (diffusive relaxation and phase slips). The stability of the Onsager dipole thus express a delicate balance where the active chirality (ω_i) pumps energy into the real, inertial modes, while the phase slips ($\beta = 1$ regime in Figure 3) provide the necessary dissipation to arrest the cascade. Equivalently, the divergence of the 3D spintronic fluid's precession inertia $\gamma \propto R^{-1}$ at the dissipative boundaries ($R \rightarrow 0$) creates a thermodynamic pressure. It is this dynamic process that acts as a thermodynamic state preparation cycle [26], mimicking coherent microwave emissions in disordered Josephson arrays [25], effectively 'pumping' the system from the high-entropy running state back into the low-entropy trapped state, thereby sustaining the Onsager dipole.

(2) the k^2 dependency in the dispersion relation corresponds to the Goldstone modes of the broken rotational symmetry (spin waves, $\omega(k) \propto k^2$). While a k^2 dependency can be modeled with odd viscosity [37], both the primary wave propagation for the Goldstone mode 'second sound' waves of Toner-Tu [9, 38] and phenomenological spin-wave models [10, 11] predict linear dispersion $\omega(k) \propto k$ (see Figure 6).

The traditional hydrodynamic modes of transfer and the spintronic waves we propose to underpin information transfer are expected to coexist in a real chiral flock. Nevertheless, we expect both regimes in which orientation (magnons) should persist when waves in density (sound) fail, and regimes where physical transport (agent velocity) poses clear limitations on the second sound propagation, but where the magnons are nevertheless able to transmit phase gradients at great speed. These cases offer ways to test the degree to which a chiral active matter is indistinguishable from a dissipative spintronic fluid.

The above notwithstanding, in our model, propagating magnons cause a high-frequency smearing that rapidly

delocalizes information. As shown in Figure 6, the dispersive nature of the magnon mode acts as an early-warning system, allowing high-frequency ‘panic’ signals to propagate through the marginally synchronized bulk well in advance of the density wavefront [39]. However, the marginal synchronization is likely realized on the spintronic fluid’s dissipative boundary, while in the ordered bulk $R \rightarrow 1$, the magnons are completely damped out. The spintronic chiral flock therefore does not turn or flow, but rather *shatters and reforms*, described in terms of shock dynamics in Ref. [8]. The Josephson inequality (Eq. 25) defines a threshold between trapped (superconducting, $|\omega - \dot{\Psi}| < I_c$) and phase-slipping (dissipative, $|\omega - \dot{\Psi}| > I_c$) turbulence. This shattering behaviour at impact is directly supported in the recent literature [40], and observations of “anomalous diffusion” during turns [39] are highly consistent with the notion of agents turning too abruptly, then phase-slip $|\omega - \dot{\Psi}| > I_c$. In the spintronic fluid, turns are initiated at the boundaries of the ordered flock where it costs almost no energy to phase-slip. This chirality is provided by the active bath ($\Delta\omega$), directly supported by Ref. [41]’s finding that turning flocks nucleate at the tips. What is more, the natural Goldstone dynamics with ferromagnetic magnons that we uncover in our model is consistent with observations of starling flocks where phase gradients travel faster than the bulk sound speed [41], as well as the paradigm of scale-free correlations in starling flocks [42].

Given the close correspondence between a spintronic fluid description and the various hydrodynamic descriptions that has accumulated, the tilted washboard potential should remain valid for many chiral active matter systems. It, and the Goldstone dynamics it drives, follow directly from the geometry of alignment itself, which, in the marginal synchronization regime, effectively forces the system to support such spin waves. Subsequently, aspects of chiral flocking, and the emergent Euler turbulence recovered in the model (Figure 1), are governed by the universality of the Landau-Lifshitz-Gilbert equation.

D. Toner-Tu theory

With spintronic chiral active matter, we provide a theoretical foundation for spin wave-models of chiral flocking. Notably, Ref. [11], where the authors explicitly introduced a phenomenological inertial spin model for starling flocks. While the chiral flock is fundamentally dissipative, the turning dynamics effectively possess inertia [10, 38], which allows for the propagation of information as spin waves [37, 43]. This is the established, robust feature of polar chiral active matter [9, 44, 45]. By deriving the phenomenon directly from the agent interaction rules, via the Adler equation and the Landau-Lifshitz-Gilbert equation, we provide a natural microscopic foundation for the concept of elasticity in Toner-Tu field theory. This microscopic foundation allows us to isolate the Josephson critical current I_c as the threshold (maximum

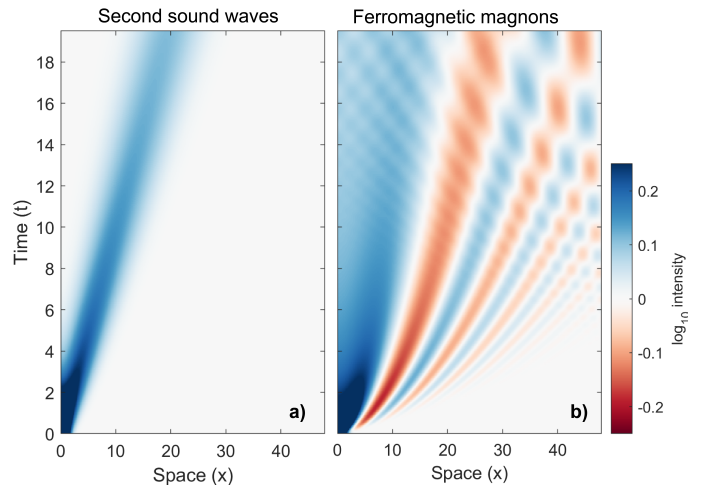


FIG. 6. **Space-time plots of a viscous hydrodynamic mode (panel a) and a ferromagnetic magnon (panel b)**, generated by first decomposing an initial Gaussian ($\sigma = 1$) signal $u(x, 0)$ into its wavenumber components $\hat{u}(k)$ using a fast Fourier transform (FFT). These components are then evolved in the frequency domain, with $\omega(k) = k - ik^2/2$ for the linear sound waves and Eq. (46) with $R = 0.2$ and $a_0 = 0.5$ for the quadratic spin waves. Finally, the evolved signal is reconstructed via an inverse FFT, $u(x, t) = \mathcal{F}^{-1}[\hat{u}(k, t)]$, and the resulting amplitude is plotted as a heatmap to visualize the transport dynamics and relative damping of both modes.

allowed turning rate of an agent) that breaks the macroscopic rigidity. When $|\omega - \dot{\Psi}| > I_c$, the fluid locally melts into the active bath, at which point the ‘second sound’ modes of Toner-Tu field theory likewise collapse. The inequality Eq. (25) may provide a quantitative threshold for the realization of flocking.

E. Topological quasiparticle gas

Ultimately, our discovery resolves the paradox of inertia in overdamped systems. In the hydrodynamic limit, Ref. [8] recovered inviscid Euler turbulence in the form of an Onsager dipole, necessitating a “phantom inertia.” In this article, we have shown that the propagation of Goldstone spin waves, caused by the azimuthal precession of the spintronic fluid, becomes mathematically indistinguishable from the advection of a massive fluid. That is, spin waves dragging phase texture along with them as they propagate constitute a topological quasi-particle.

Interestingly, these quasi-particles interact via the long-range field interaction of the Kirchhoff-Onsager Hamiltonian [8] rather than via local collisions. This is consistent with the recognized proliferation of self-propelled topological defects in active nematics [46], where defect cores are the sites of maximum stress and energy dissipation [47], leading to inverse cascades [48, 49].

F. Disorder as source of order

The implications of our model is that wide tracts of stochastic noise are causally connected to complex large-scale features. A marginal R yields a dispersion relation (Eq. 46) that enables fast, strong and frequency-dispersed magnons to propagate (Figure 6), and the frustration $\Delta\omega$ works both to lower R and to keep the agents constantly precessing around the tilted washboard potential (Figure 5b). This notion, which may spawn future beneficial applications of fabrication heterogeneity, is consistent with observations from nature.

In biological terms, the stress, or frustration $\Delta\omega$, corresponds to phenotypic heterogeneity [15, 50], noisy genetic expression. The system manages this noise by physically segregating phase conflicts into discrete, topologically protected defect cores. This segregation leaves the bulk in a critical state of marginal synchronization ($0 < R < 1$), accessible only in the negative-temperature regime of a bounded vortex gas [8]. Thus, the flock’s capacity to “twist”, or propagating order via spin waves, is strictly contingent on a sufficiently *wide* noise expression $\Delta\omega$.

Given the complete isomorphism between our minimalist model and disordered Josephson junction theory, our assertion that *noise* optimizes a system by pushing it towards criticality is supported by research into non-equilibrium quantum thermodynamics [25, 26], providing an avenue for spintronics to accurately model active matter.

It is important, however, to stress that the formal isomorphism to the standard resistively shunted junction model, and the subsequent recovery of overdamped spintronics via the Landau-Lifshitz-Gilbert equation, strictly relies on the polar symmetry of the interaction (flocking, [51]). nematic active matter exhibits half-integer symmetry and would imply a π -periodic potential [52] that maps to distinct universality classes (e.g., XY_2 models [53]), unable to support the integer vortex topology of the Onsager dipole. In contrast, the 2π -periodicity of the polar alignment interaction, $-\sin(\phi_i - \Psi)$, must map directly to the sinusoidal current-phase relation of a superconducting tunnel junction [16, 17].

The key insight from our results lies in the origin of the description we have elucidated in this section. The 3D geometric constraints of polar, chiral particles lead directly to the two-dimensional motile Kuramoto model (Figure 4) and are entirely isomorphic to Gilbert damping in a magnetic field. The reason for this convergence is that both spintronics and chiral active matter obey the universality of the Landau-Lifshitz-Gilbert equation. Chiral active matter must, therefore, be strictly considered as a dissipative spintronic fluid, where the active bath at the boundaries provides the thermodynamic pressure that stabilizes the inertial bulk.

VII. CONCLUSION

We have derived a strict isomorphism between a minimalist, two-dimensional chiral active matter model, and resistively shunted junction theory, by recovering the Adler equation in the model’s dynamics (Eq. 9). We subsequently followed the formalism developed by Ref. [22] for individual disordered Josephson junctions, thereby demonstrating that the system is governed by a tilted washboard potential. A thermodynamic transition separates resistive ‘running’ agents from the ‘trapped’ population, the latter of which explicitly sustain an information supercurrent.

By extending the model to three dimensions, we recovered the Landau-Lifshitz-Gilbert equation for an overdamped spintronic fluid. The information supercurrents that we have predicted and described in empirical terms transmit phase gradients across the chiral flock, sustaining Goldstone modes from the precession around the mean field of the 3D active bath. The resulting spin waves advect phase gradients, providing inertia to the inviscid Euler turbulence of the Onsager dipole. The “phantom inertia” discovered in Ref. [8], $\lambda = R^2$, is therefore physically identified as the precession stiffness of the order parameter in three dimensions.

If substantiated in future forays, the transition to active chiral turbulence must be considered the emergence of a topological quasiparticle gas, where macroscopic Onsager dipoles, in turn bound states of phase singularities, acquire effective inertia from the Goldstone modes (azimuthal precession) of the underlying broken symmetry.

ACKNOWLEDGEMENTS

This work is supported by the European Space Agency’s Living Planet Grant No. 1000012348. The author is grateful to O. Nestande, D. Knudsen, PT. Jayachandran, and K. Douch for stimulating discussions. Google’s Gemini 3.0 Pro has been used for mathematical formalism and coding assistance in MATLAB.

APPENDIX A: DERIVING THE DISPERSION RELATION

We consider the spin waves supported by the azimuthal turning inertia and perturb the ordered state, linearizing the polarized state around small perturbations to $\hat{n}(\mathbf{r}, t)$. That is, a flock perfectly aligned along the z -axis with a small perturbation \mathbf{m} in the xy -plane:

$$\hat{n}(\mathbf{r}, t) \approx \hat{z} + \mathbf{m}(\mathbf{r}, t) \quad \text{where} \quad \mathbf{m} = (m_x, m_y, 0), \quad (34)$$

which we shall eventually insert into Eq. (30).

Neglecting higher-order terms ($|\mathbf{m}|^2 \approx 0$), the Laplacian is $\nabla^2 \hat{n} \approx (\nabla^2 m_x, \nabla^2 m_y, 0)$. We now evaluate the cross products to first order in \mathbf{m} :

$$\hat{z} \times \nabla^2 \mathbf{m} = \nabla^2 m_x \hat{y} - \nabla^2 m_y \hat{x}, \quad (35)$$

and,

$$\hat{z} \times (\hat{z} \times \nabla^2 \mathbf{m}) = -\nabla^2 \mathbf{m}. \quad (36)$$

The former corresponds to inertial precession, while the latter leads to alignment. Substituting these expressions back into the extended equation:

$$\frac{\partial \mathbf{m}}{\partial t} = -\frac{a_0 \xi^2}{R} (\nabla^2 m_x \hat{y} - \nabla^2 m_y \hat{x}) + (a_0 R \xi^2) \nabla^2 \mathbf{m}. \quad (37)$$

Separating into vector components yields:

$$\dot{m}_x = \frac{a_0 \xi^2}{R} \nabla^2 m_y + (a_0 R \xi^2) \nabla^2 m_x, \quad (38)$$

$$\dot{m}_y = -\frac{a_0 \xi^2}{R} \nabla^2 m_x + (a_0 R \xi^2) \nabla^2 m_y. \quad (39)$$

Proposing a plane wave solution $\mathbf{m} \sim e^{i(kx - \omega t)}$ (with

$\partial_t \rightarrow -i\omega$ and $\nabla^2 \rightarrow -k^2$), the coupled equations read:

$$-i\omega m_x = -\frac{a_0 \xi^2}{R} k^2 m_y - (a_0 R \xi^2) k^2 m_x, \quad (40)$$

$$-i\omega m_y = +\frac{a_0 \xi^2}{R} k^2 m_x - (a_0 R \xi^2) k^2 m_y. \quad (41)$$

Rearranging into matrix form $\mathbf{Mm} = 0$:

$$\begin{pmatrix} -i\omega + (a_0 R \xi^2) k^2 & \frac{a_0 \xi^2}{R} k^2 \\ -\frac{a_0 \xi^2}{R} k^2 & -i\omega + (a_0 R \xi^2) k^2 \end{pmatrix} \begin{pmatrix} m_x \\ m_y \end{pmatrix} = 0. \quad (42)$$

For non-trivial solutions, the determinant must be zero:

$$(-i\omega + a_0 R \xi^2 k^2)^2 + \left(\frac{a_0 \xi^2}{R} k^2 \right)^2 = 0. \quad (43)$$

Solving for ω :

$$-i\omega + a_0 R \xi^2 k^2 = \mp i \frac{a_0 \xi^2}{R} k^2, \quad (44)$$

$$\omega(k) = \pm \frac{a_0 \xi^2}{R} k^2 - i(a_0 R \xi^2) k^2. \quad (45)$$

Absorbing the interaction scale ξ^2 into the normalization (or setting $\xi = 1$), we recover the final dispersion relation:

$$\omega(k) = \pm \frac{a_0}{R} k^2 - i(a_0 R) k^2. \quad (46)$$

-
- [1] H. H. Wensink, J. Dunkel, S. Heidenreich, K. Drescher, R. E. Goldstein, H. Löwen, and J. M. Yeomans, Mesoscale turbulence in living fluids, *Proceedings of the National Academy of Sciences* **109**, 14308 (2012).
- [2] I. S. Aranson, Bacterial active matter, *Reports on Progress in Physics* **85**, 076601 (2022).
- [3] R. Alert, J. Casademunt, and J.-F. Joanny, Active Turbulence, *Annual Review of Condensed Matter Physics* **13**, 143 (2022).
- [4] M. Bourgoïn, R. Kervil, C. Cottin-Bizonne, F. Raynal, R. Volk, and C. Ybert, Kolmogorovian Active Turbulence of a Sparse Assembly of Interacting Marangoni Surfers, *Physical Review X* **10**, 021065 (2020).
- [5] K. Qi, E. Westphal, G. Gompper, and R. G. Winkler, Emergence of active turbulence in microswimmer suspensions due to active hydrodynamic stress and volume exclusion, *Communications Physics* **5**, 49 (2022).
- [6] D. Saintillan and M. J. Shelley, Active suspensions and their nonlinear models, *Comptes Rendus Physique Living Fluids / Fluides Vivants*, **14**, 497 (2013).
- [7] J. K. Bhattacharjee and T. R. Kirkpatrick, Activity induced turbulence in driven active matter, *Physical Review Fluids* **7**, 034602 (2022).
- [8] M. F. Ivarsen, Onsager Condensation in Chiral Active Matter: Universality of Supersonic Topological Gas Dynamics (2025), arXiv:2512.01884 [cond-mat].
- [9] J. Toner and Y. Tu, Flocks, herds, and schools: A quantitative theory of flocking, *Physical Review E* **58**, 4828 (1998).
- [10] X. Yang and M. C. Marchetti, Hydrodynamics of Turning Flocks, *Physical Review Letters* **115**, 258101 (2015).
- [11] A. Cavagna, L. Del Castello, I. Giardina, T. Grigera, A. Jelic, S. Melillo, T. Mora, L. Parisi, E. Silvestri, M. Viale, and A. M. Walczak, Flocking and Turning: A New Model for Self-organized Collective Motion, *Journal of Statistical Physics* **158**, 601 (2015).
- [12] M. F. Ivarsen, Kinetic Turing Instability and Emergent Spectral Scaling in Chiral Active Turbulence (2025), arXiv:2508.21012 [physics].
- [13] J. A. Acebrón, L. L. Bonilla, C. J. Pérez Vicente, F. Ritort, and R. Spigler, The Kuramoto model: A simple paradigm for synchronization phenomena, *Reviews of Modern Physics* **77**, 137 (2005).
- [14] F. De Smet and D. Aeyels, Partial entrainment in the finite Kuramoto-Sakaguchi model, *Physica D: Nonlinear Phenomena* **234**, 81 (2007).
- [15] M. Ackermann, A functional perspective on phenotypic heterogeneity in microorganisms, *Nature Reviews Microbiology* **13**, 497 (2015).
- [16] B. D. Josephson, Possible new effects in superconductive tunnelling, *Physics Letters* **1**, 251 (1962).
- [17] M. Tinkham, *Introduction to Superconductivity* (Courier

- Corporation, 2004).
- [18] K. Wiesenfeld, P. Colet, and S. H. Strogatz, Synchronization Transitions in a Disordered Josephson Series Array, *Physical Review Letters* **76**, 404 (1996).
- [19] V. Ambegaokar and B. I. Halperin, Voltage Due to Thermal Noise in the dc Josephson Effect, *Physical Review Letters* **22**, 1364 (1969).
- [20] W. C. Stewart, Current-Voltage Characteristics of Josephson Junctions, *Applied Physics Letters* **12**, 277 (1968).
- [21] D. E. McCumber, Effect of ac Impedance on dc Voltage-Current Characteristics of Superconductor Weak-Link Junctions, *Journal of Applied Physics* **39**, 3113 (1968).
- [22] L. Danner, C. Padurariu, J. Ankerhold, and B. Kubala, Injection locking and synchronization in Josephson photonics devices, *Physical Review B* **104**, 054517 (2021).
- [23] Y. Fang, S. Han, S. Chesi, and M.-S. Choi, Subgap modes in two-dimensional magnetic Josephson junctions, *Physical Review B* **107**, 115114 (2023).
- [24] M. Y. Marov and A. V. Kolesnichenko, Self-Organization of Developed Turbulence and Formation Mechanisms of Coherent Structures, in *Turbulence and Self-Organization: Modeling Astrophysical Objects*, edited by M. Y. Marov and A. V. Kolesnichenko (Springer, New York, NY, 2013) pp. 373–423.
- [25] S. P. Benz and C. J. Burroughs, Coherent emission from two-dimensional Josephson junction arrays, *Applied Physics Letters* **58**, 2162 (1991).
- [26] C. Kurtscheid, A. Redmann, F. Vewinger, J. Schmitt, and M. Weitz, Thermodynamics and State Preparation in a Two-State System of Light, *Physical Review Letters* **135**, 160406 (2025).
- [27] P. Bhansali and J. Roychowdhury, Gen-Adler: The generalized Adler’s equation for injection locking analysis in oscillators, in *2009 Asia and South Pacific Design Automation Conference* (2009) pp. 522–527.
- [28] P. Gandhi, E. Knobloch, and C. Beaume, Dynamics of phase slips in systems with time-periodic modulation, *Physical Review E* **92**, 062914 (2015).
- [29] K. K. Likharev, *Dynamics of Josephson Junctions and Circuits* (Routledge, London, 1986).
- [30] R. S. Newrock, C. J. Lobb, U. Geigenmüller, and M. Octavio, The two-dimensional physics of Josephson junction arrays, in *Solid State Physics*, Vol. 54 (Elsevier, 2000) pp. 263–512.
- [31] G. F. Carnevale, J. C. McWilliams, Y. Pomeau, J. B. Weiss, and W. R. Young, Evolution of vortex statistics in two-dimensional turbulence, *Physical Review Letters* **66**, 2735 (1991).
- [32] V. D. Larichev and J. C. McWilliams, Weakly decaying turbulence in an equivalent-barotropic fluid, *Physics of Fluids A: Fluid Dynamics* **3**, 938 (1991).
- [33] J. D’Errico, SLM-shape language modeling, SLM-Shape Language Modeling. <http://www.mathworks.com/matlabcentral/fileexchange/24443-slm-shape-language-modeling>: Mathworks (2009).
- [34] M. Lakshmanan, The fascinating world of the Landau–Lifshitz–Gilbert equation: An overview, *Philosophical Transactions of the Royal Society A: Mathematical, Physical and Engineering Sciences* **369**, 1280 (2011).
- [35] M. Johnson and R. H. Silsbee, Interfacial charge-spin coupling: Injection and detection of spin magnetization in metals, *Physical Review Letters* **55**, 1790 (1985).
- [36] G.-L. Ingold, H. Grabert, and U. Eberhardt, Cooper-pair current through ultrasmall Josephson junctions, *Physical Review B* **50**, 395 (1994).
- [37] T. Markovich and T. C. Lubensky, Odd Viscosity in Active Matter: Microscopic Origin and 3D Effects, *Physical Review Letters* **127**, 048001 (2021).
- [38] L. P. Dadhichi, J. Kethapelli, R. Chajwa, S. Ramaswamy, and A. Maitra, Nonmutual torques and the unimportance of motility for long-range order in two-dimensional flocks, *Physical Review E* **101**, 052601 (2020).
- [39] A. Cavagna, S. M. D. Queirós, I. Giardina, F. Stefanini, and M. Viale, Diffusion of individual birds in starling flocks, *Proceedings of the Royal Society B: Biological Sciences* **280**, 20122484 (2013).
- [40] P. W. Miller and N. T. Ouellette, Impact fragmentation of model flocks, *Physical Review E* **89**, 042806 (2014).
- [41] A. Attanasi, A. Cavagna, L. Del Castello, I. Giardina, T. S. Grigera, A. Jelić, S. Melillo, L. Parisi, O. Pohl, E. Shen, and M. Viale, Information transfer and behavioural inertia in starling flocks, *Nature Physics* **10**, 691 (2014).
- [42] A. Cavagna, A. Cimorelli, I. Giardina, G. Parisi, R. Santagati, F. Stefanini, and M. Viale, Scale-free correlations in starling flocks, *Proceedings of the National Academy of Sciences* **107**, 11865 (2010).
- [43] A. Cavagna, J. Cristín, I. Giardina, T. S. Grigera, and M. Veca, Discrete Laplacian thermostat for flocks and swarms: The fully conserved Inertial Spin Model, *Journal of Physics A: Mathematical and Theoretical* **57**, 415002 (2024).
- [44] B. Mahault, F. Ginelli, and H. Chaté, Quantitative Assessment of the Toner and Tu Theory of Polar Flocks, *Physical Review Letters* **123**, 218001 (2019).
- [45] L. Caprini, B. Liebchen, and H. Löwen, Self-reverting vortices in chiral active matter, *Communications Physics* **7**, 153 (2024).
- [46] S. Shankar, A. Souslov, M. J. Bowick, M. C. Marchetti, and V. Vitelli, Topological active matter, *Nature Reviews Physics* **4**, 380 (2022).
- [47] L. Giomi, Geometry and Topology of Turbulence in Active Nematics, *Physical Review X* **5**, 031003 (2015).
- [48] A. Doostmohammadi, M. F. Adamer, S. P. Thampi, and J. M. Yeomans, Stabilization of active matter by flow-vortex lattices and defect ordering, *Nature Communications* **7**, 10557 (2016).
- [49] G. Spera, J. M. Yeomans, and S. P. Thampi, Low-Pass Filtering of Active Turbulent Flows to Liquid Substrates (2025), arXiv:2511.22701 [cond-mat].
- [50] G. Ariel, A. Rabani, S. Benisty, J. D. Partridge, R. M. Harshey, and A. Be’er, Swarming bacteria migrate by Lévy Walk, *Nature Communications* **6**, 8396 (2015).
- [51] T. Vicsek, A. Czirók, E. Ben-Jacob, I. Cohen, and O. Shochet, Novel Type of Phase Transition in a System of Self-Driven Particles, *Physical Review Letters* **75**, 1226 (1995).
- [52] M. C. Marchetti, J. F. Joanny, S. Ramaswamy, T. B. Liverpool, J. Prost, M. Rao, and R. A. Simha, Hydrodynamics of soft active matter, *Reviews of Modern Physics* **85**, 1143 (2013).
- [53] F. C. Poderoso, J. J. Arenzon, and Y. Levin, New Ordered Phases in a Class of Generalized $\$XY\$$ Models, *Physical Review Letters* **106**, 067202 (2011).